ACS OMEGA

http://pubs.acs.org/journal/acsodf

Article

# Impact of Hydrogen Coverage Trend on Methyl Formate Adsorption on $MoS_2$ Surface: A First Principles Study

Samuel E. P. P. Masan, Febdian Rusydi,* Wahyu A. E. Prabowo, Daniel Elisandro, Wun F. Mark-Lee, Nabila A. Karim, and Adhitya G. Saputro

Cite This: *ACS Omega* 2023, 8, 6523−6529

Read Online

ACCESS | Metrics & More | Article Recommendations | Supporting Information

**ABSTRACT:** Adsorbates coverage plays a crucial role in a catalysis reaction. In hydrodeoxygenation (HDO), which involves high hydrogen pressure, hydrogen coverage on the surface may affect the adsorption of other adsorbates. The HDO is used in green diesel technology to produce clean and renewable energy from organic compounds. This motivates us to study the hydrogen coverage effect on methyl formate adsorption on $MoS_2$ as a model case of the actual HDO. We calculate the methyl formate adsorption energy as a function of hydrogen coverage using density functional theory (DFT) and then comprehensively analyze the physical origin of the results. We find that methyl formate can have several adsorption modes on the surface. The increased hydrogen coverage can stabilize or destabilize these adsorption modes. However, finally, it leads to convergence at high hydrogen coverage. We extrapolated the trend further and concluded that some adsorption modes might not exist at high hydrogen coverage, while others remain.

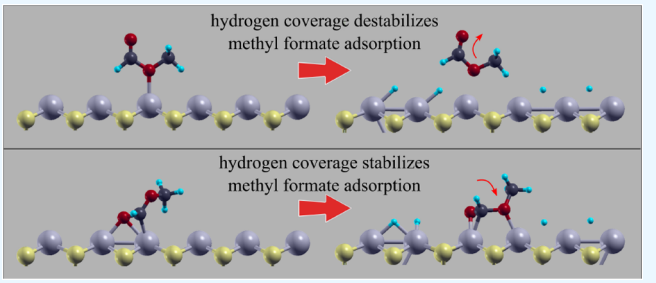




## INTRODUCTION

Adsorption on a catalyst surface is an important step in heterogeneous catalysis. If adsorption is too weak, catalysis may not occur. On the other hand, if adsorption is too strong, the final product cannot be achieved. This is the well-known Sabatier principle.[1] It has motivated many fundamental studies about adsorption on surfaces.[2−5]

Moreover, interactions between adsorbates could also influence catalysis. This is commonly known as the coverage effect. On monometallic catalysts, the coverage effect has been intensively studied. Changes in coverage may affect molecule adsorption and later change the reaction rate and selectivity.[6−8] On the other hand, the studies on the coverage effect on transition metal dichalcogenide (TMD) materials are limited. The coverage effect on TMD may differ from that on monometallic catalysts. For instance, Huang et al. reported that methyl formate hydrogenolysis rates on a copper-based catalyst have a positive order for hydrogen.[9] This means that an increase in hydrogen pressure, which corresponds to an increase in hydrogen coverage, will raise the reaction rate. Interestingly, Wang et al. reported the opposite trend for hydrodeoxygenation (HDO) of *p*-cresol on $MoS_2$.[10]

There are several works that discuss the effect of hydrogen coverage on $MoS_2$. For instance, Grønborg et al. studied the hydrogen-induced reshaping and edge activation of $MoS_2$.[11] Kronberg et al. studied the hydrogen coverage effect on the hydrogen adsorption on $MoS_2$.[12] Rosen et al. studied the $MoS_2$ stability under the reaction condition in which high-pressure $H_2$ and $H_2S$ are involved.[13] Nevertheless, studies about the hydrogen coverage effect on the adsorption of an oxygenated molecule are still scarce.

In this work, we report the hydrogen coverage effect on the adsorption of the oxygenated molecule on $MoS_2$ using density functional theory (DFT) calculation. We choose methyl formate as the oxygenated molecule since it has the same ester functional group as triglyceride, commonly used as raw material in HDO for green diesel production.[14−17] Moreover, several recent works also used methyl formate in triglyceride interesterification for biodiesel production.[18,19] We only consider the perfect Mo-edge of $MoS_2$ (see left panel of Figure 1) since adsorption on the other edge (S-edge) is weaker for both hydrogen[12] and ester molecules.[20] Note that under reaction conditions the perfect Mo-edge may be saturated with sulfur atoms, rendering it unreactive.[13] However, this sulfur coverage is not discussed in this work and has yet to be investigated.

**Received:** October 26, 2022
**Accepted:** February 2, 2023
**Published:** February 13, 2023

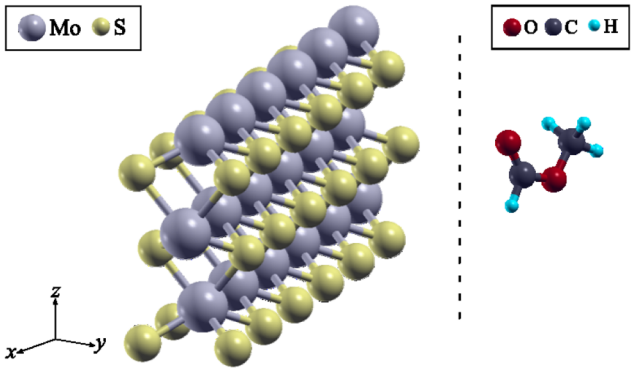


**Figure 1.** Mo-edge $MoS_2$ surface (left) and methyl formate molecule (right) used in this work.

## COMPUTATIONAL DETAILS

We carried out DFT calculations using the Quantum ESPRESSO package.[21,22] We modeled the core electrons using Plane Augmented Wave function[23] and described the exchange−correlation functional using the generalized gradient approximation Perdew−Burke−Ernzerhof (PBE).[24] We also took into account the dispersion correction using Grimme-d2.[25] The optimized $MoS_2$ structural parameters given by these models are $a_0$ = 3.188 Å and $c_0$ = 12.332 Å, which are in good agreement with the reported experimental value ($a_0$ = 3.160 Å and $c_0$ = 12.294 Å).[26]

Other calculation details are reported as follows. To sample the Brillouin zone, we used a 3 × 1 × 1 Monkhorst−Pack k-point grid.[27] We chose a 500 eV kinetic energy cutoff ($E_{cutoff}$) for the wave function. The rationale for the k-point and $E_{cutoff}$ values can be found in Figure S1 and Figure S2. We set a $10^{-6}$ Ry energy threshold for self-consistent field calculation. We performed the geometry optimization based on the Broyden−Fletcher−Goldfarb−Shanno quasi-Newton algorithm[28] until the force was smaller than $10^{-3}$ Ry/bohr. Moreover, we analyzed the system's density of states (DOS) by projecting them into an atomic and molecular orbital. An explanation of the latter is provided by Ravikumar et al.[29] We calculated the transition barrier between one atomic environment to another using the climbing image nudged elastic band method.[30] Finally, we calculated the atomic charge density using the Bader Charge Analysis package.[31]

We used the same slab model for Mo-edge $MoS_2$ as in ref 20. The slab consists of 36 S atoms and 18 Mo atoms, forming three layers as shown in the left panel of Figure 1. Only the uppermost layer is relaxed during the geometry optimization, while the other two are fixed in the bulk structure. To prevent the interaction between the periodic boundary condition, we set at least 16 Å vacuum in the $z$ axis after performing a convergence test (see Figure S3). The resulting slab's dimension is 18.97 Å × 12.30 Å × 21.28 Å. This slab has six Mo-top and six Mo−Mo-bridge sites which are considered the active site in this work.

We used the cis conformer of methyl formate as the initial structure before adsorption (see right panel of Figure 1). This conformer is the most stable one at room temperature.[32,33] We also confirmed this by comparing the energy of cis conformer with another stable conformer, i.e., trans. Our DFT calculation shows that the energy of the cis conformer is 0.19 eV lower than that of trans.

We defined the adsorption energy as the energy difference between the adsorbed and isolated atom/molecule. The more negative the value, the stronger the adsorption is. We calculated hydrogen and methyl formate adsorption energy using equations 1 and 2, respectively. In those equations, MF, $n$H, and surf refer to methyl formate, the number of adsorbed hydrogen atoms, and $MoS_2$, respectively. Moreover, we defined the hydrogen coverage by comparing $n$H with six Mo-top or six Mo−Mo-bridge sites available on the slab (see equation 3).

$$E_{ads\text{-}H} = E_{n\mathrm{H,surf}} - (nE_{\mathrm{H}} + E_{surf}) \quad (1)$$

$$E_{ads\text{-}MF} = E_{\mathrm{MF},n\mathrm{H,surf}} - (E_{\mathrm{MF}} + E_{n\mathrm{H,surf}}) \quad (2)$$

$$\theta_{\mathrm{H}} = \frac{n\mathrm{H}}{6} \quad (3)$$

## RESULTS AND DISCUSSION

**Hydrogen Adsorption.** A single hydrogen atom can be adsorbed on Mo-top and Mo−Mo-bridge sites of Mo-edge $MoS_2$. The adsorption energies on both sites are −0.67 and −1.00 eV, respectively. These adsorption sites may be provided by $d_{z^2}$ (on Mo-top) and $d_{xz}$ (on Mo−Mo-bridge) bands of the Mo atoms (see peaks A and C in Figure 2). The $d_{z^2}$ peak is located just below the Fermi level, while $d_{xz}$ is about −0.2 eV lower. The difference results in a more stable bonding between the s orbital of the hydrogen atom and the $d_{xz}$ band on Mo−Mo-bridge.[2] Moreover, compared to $d_{z^2}$, $d_{xz}$ has a higher electron density near the Fermi level which will be transferred to the adsorbate. These explain why the hydrogen atom prefers to be adsorbed on Mo−Mo-bridge more than on Mo-top. At higher hydrogen coverage ($\theta_{\mathrm{H}}$ > 16.7%), hydrogen atoms tend to be adsorbed on the most stable site, i.e., Mo−Mo-bridge. Some hydrogen atoms can be adsorbed on Mo-top only until 66.67% coverage. More than that, all hydrogen atoms are adsorbed on Mo−Mo-bridge.

The geometry of $MoS_2$ is almost unchanged upon hydrogen adsorption on Mo-top, while the opposite is true for hydrogen adsorption on Mo−Mo-bridge. On Mo−Mo-bridge, hydrogen attracts its nearest neighbor Mo atoms causing the Mo−Mo distance to be reduced by 0.38 Å. We argue that this geometrical change is important in the hydrogen-induced $MoS_2$ reshaping observed in scanning tunneling microscopy (STM).[11] The geometrical change suggests that some internal bonds of $MoS_2$ are getting stronger while other are getting weaker. The change can trigger the reshaping of $MoS_2$ (for instance, bigger structures decompose into several smaller structures). This process is similar to transition metal surface reconstruction which involved subsurface adsorption of hydrogen and oxygen atoms.[34,35]

The hydrogen adsorption generally destabilizes as the coverage increases; i.e., the adsorption energy increases (see Figure 3). This trend agrees with a previous study by Kronberg et al. which calculates the average of hydrogen adsorption energy as a function of hydrogen coverage on $MoS_2$.[12] However, since adsorption is site-dependent, the trend is not always valid. For instance, we observed that at 33.3% coverage, the trend changed into stabilization when the interatomic distance between the adsorbed hydrogen atoms increased by 3.32 Å (see insets of Figure 3). The change between these two atomic environments depicts a hydrogen diffusion with an energy barrier of 0.16 eV (see Figure S6). This barrier is significantly lower than the diffusion barrier of a single



https://doi.org/10.1021/acsomega.2c06888
ACS Omega 2023, 8, 6523−6529

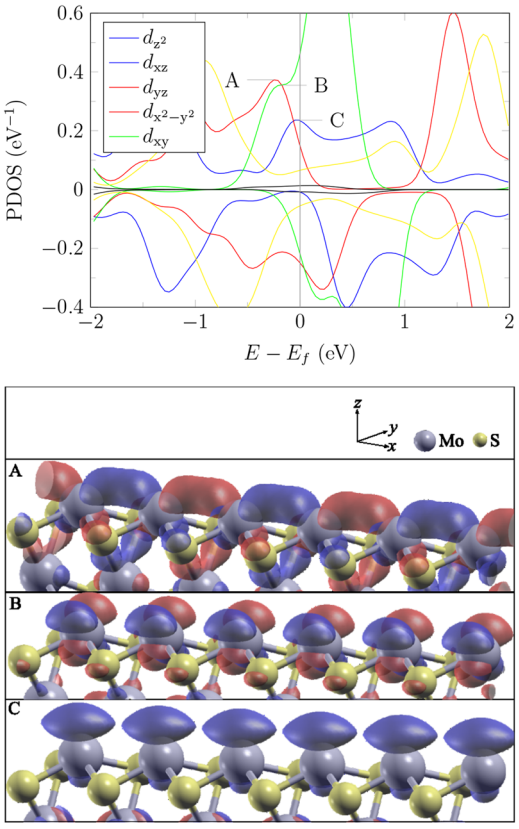


**Figure 2.** Top panel: the projected density of states (PDOS) of Mo atom's d bands on Mo-edge $MoS_2$. The energy in the horizontal axis is relative to the Fermi level. The positive and negative values of PDOS correspond to spin up and down, respectively. There are three d band peaks near the Fermi level (peaks A, B, and, C) which may host adsorption on $MoS_2$. Bottom panel: wave function isosurface at energy levels A, B, and C of the top panel figure. The isovalue is 0.0006. Blue and red colors represent positive and negative phases, respectively. Peaks A and C host hydrogen adsorption, while peaks A, B, and C host methyl formate adsorption.

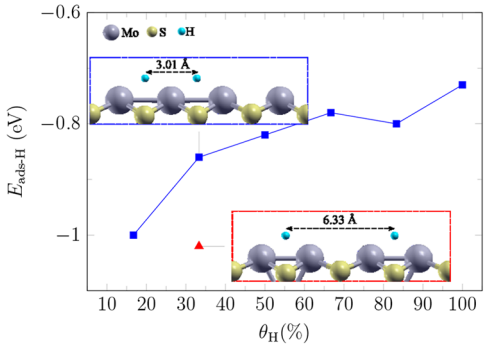


**Figure 3.** Plot of hydrogen adsorption energy ($E_{ads-H}$) on Mo−Mo-bridge as a function of hydrogen coverage ($\theta_H$). For the rectangle marks, we put hydrogen atoms on successive Mo−Mo-bridge sites. For the triangle mark, there is an empty Mo−Mo-bridge site between the two adsorbed hydrogen atoms. The visualization of adsorptions at 33% coverage are shown in the inset.

adsorbed hydrogen ($\theta_H$ = 0.16%), which is 0.32 eV. The change in adsorption energy and diffusion barrier show that there should be a repulsive interaction between the adsorbed hydrogen atoms. Our Bader charge analysis suggests that this should come from Coulombic repulsion since hydrogen possesses excess electrons after adsorption (see Table S1).

**Methyl Formate Adsorption.** There are at least six methyl formate adsorption modes on Mo-edge $MoS_2$ (see Figure 4). The density of states (DOS) analysis reveals that the methyl formate molecular orbital undergoes hybridization in all six adsorption modes (see Figure S4). The hybridization implies that all adsorption modes are chemisorption.

Generally, methyl formate adsorption on Mo-top ($\mu_1$) is stronger than on Mo−Mo-bridge ($\mu_2$). The adsorption energy of $\eta_1\mu_1$ is 0.1 eV more negative than that of $\eta_1\mu_2$. The same trend is also observed in $\eta_2\mu_1$ and $\eta_2\mu_2$. This trend is interestingly contradicted by hydrogen, which prefers $\mu_2$ than $\mu_1$ mode (see section Hydrogen Coverage Effect on Methyl Formate Adsorption). The contradiction arises from the difference in the frontier orbital symmetry between hydrogen and methyl formate. The symmetry of the Highest Occupied Molecular Orbital (HOMO) and the Lowest Unoccupied Molecular Orbital (LUMO) (see Figure 5) allow them to interact strongly with the Mo atom's $d_{xz}$ and $d_{yz}$ bands (see peaks A and B in Figure 2) via adsorption on Mo-top. On the other hand, there should be only a weak interaction on Mo−Mo-bridge. We provide a schematic to explain the interaction of methyl formate molecular orbitals with Mo d bands in Figure 6.

In the $\eta_1$ modes ($\eta_1\mu_1$*, $\eta_1\mu_1$, and $\eta_1\mu_2$), methyl formate is only adsorbed through its oxygen atoms. These $\eta_1$ modes are also observed in the other oxygenated molecules that adsorbed on $MoS_2$[20,36−38] and other transition metal surfaces.[39] Adsorptions through the oxygen of the carbonyl group (C═O) are 0.2 eV stronger than that of the ether group (C−O−C). This trend agrees with the adsorption of methyl propionate,[38] which is assigned to the higher nucleophilic character of the oxygen of the C═O group.

The $\eta_2$ and $\eta_3$ modes involve the adsorption of the C═O group. These adsorptions happen through $\pi$ back-donation, as shown in Figure 7. The shift of the HOMO and LUMO to the right and left of the Fermi level indicates some electron exchange between methyl formate and $MoS_2$. Methyl formate donates electrons from its HOMO. In return, $MoS_2$ gives a back-donation to methyl formate's LUMO. The LUMO is mainly formed by the $\pi$* orbital of the C═O group (see Figure 5). Back-donation to this $\pi$* orbital caused the C═O bond elongation for more than 0.1 Å (see Table S3).

**Hydrogen Coverage Effect on Methyl Formate Adsorption.** We note that generally, hydrogen coverage strongly affects methyl formate adsorption energy, as shown in Figure 8. The increased hydrogen coverage either stabilizes or destabilizes methyl formate adsorption. Similar to our discussion in the previous subsection about hydrogen adsorption, we suggest that this effect may come from Coulombic interaction since methyl formate and hydrogen are negatively charged on the $MoS_2$ surface (see Bader charge analysis in Table S1 and Table S2). The rest of this subsection will focus on discussing the trend in Figure 8.

For $\eta_1$ modes, increased hydrogen coverage first stabilizes the methyl formate adsorption energy by about −0.4 eV but later slowly destabilizes it. The stabilization happens because the Coulombic interaction with hydrogen forces methyl formate toward a more stable adsorption configuration. For instance, $\eta_1\mu_2$ transforms into $\eta_1\mu_1$ mode, which is more stable (see Figure S5). This may provide a good explanation for the


https://doi.org/10.1021/acsomega.2c06888
ACS Omega 2023, 8, 6523−6529

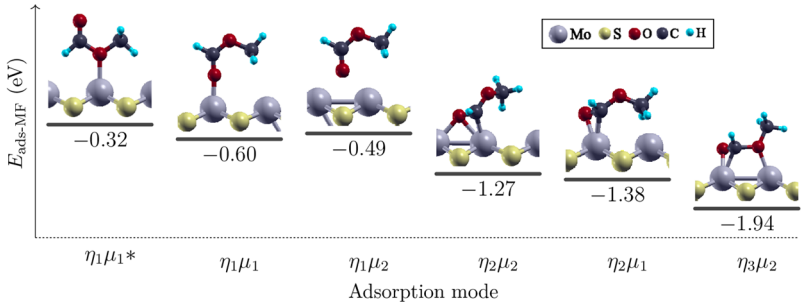


**Figure 4.** Energy level diagram of all methyl formate adsorption modes on Mo-edge $MoS_2$. The $\eta_x\mu_y$ refers to $x$ number of atoms in adsorbate, which is adsorbed through $y$ number of atoms on the surface. Since there are two $\eta_1\mu_1$ modes, we mark the less stable one with * to distinguish them.

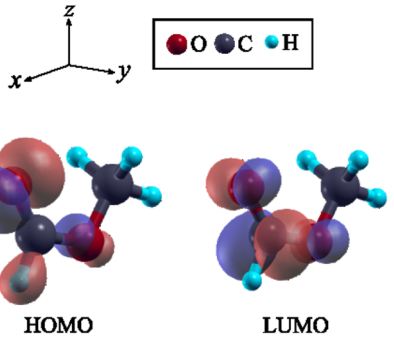


**Figure 5.** Isosurface of HOMO and LUMO of methyl formate. The isovalue is 0.006. Blue and red colors represent positive and negative phases, respectively.

similar trends reported by Valencia et al.[40] for organic compound adsorption on the $MoO_3$ surface.

Compared to $\eta_1$, hydrogen coverage has a smaller effect on $\eta_2$ adsorption energy. At 33.3% hydrogen coverage, $\eta_2$ adsorption energy changes by about ±0.2 eV. It later stabilizes by about −0.2 eV at higher coverage ($\theta_H$ = 66.7%). Geometrically, the stabilization is especially noticeable for the $\eta_2\mu_2$ mode, which transforms into $\eta_3\mu_2$ (see Figure S5).

Interestingly, the most stable adsorption ($\eta_3$) is strongly affected by hydrogen coverage. Since it is already in the most stable adsorption state, Coulombic repulsion from the surrounding hydrogen can only destabilize it. The adsorption energy is increased by +0.12 eV at 33.3% coverage and then by +0.31 eV more at 66.7% coverage.

In the time scale of experiments, one adsorption mode may change to another. For the most favorable change, which is $\eta_1\mu_1$* into $\eta_3\mu_2$, NEB calculations show that the higher the hydrogen coverage, the higher the energy barrier of the change (see Figure S7). For 66.7% hydrogen coverage, the energy barrier (0.38 eV) becomes higher than the $\eta_1\mu_1$* desorption energy (0.20 eV). These results imply that, under high hydrogen coverage, it is likely for $\eta_1\mu_1$* to desorb than to change to another stabler adsorption mode.

Finding the most stable adsorption mode of methyl formate prior to the investigation of HDO catalytic reaction is crucial. The extrapolation of our results in Figure 8 suggests that the $\eta_1$ mode leads the methyl formate to desorb under high hydrogen pressure. The desorption decreases the number of methyl formate adsorbed on $MoS_2$, which may lead to the decreasing HDO activity on $MoS_2$ at high hydrogen pressure, as reported by Wang et al.[10] While the ester in the $\eta_1$ mode tends to desorb, the one with $\eta_2$ and $\eta_3$ converges to a similar mode in higher hydrogen coverage with an adsorption energy around −1.5 eV. The adsorption energy is strong enough to ensure methyl formate stays on the $MoS_2$ surface for pursuing a further reaction stage.

## CONCLUSIONS

We used DFT calculations to study the effect of hydrogen coverage on methyl formate adsorption over a perfect Mo-edge

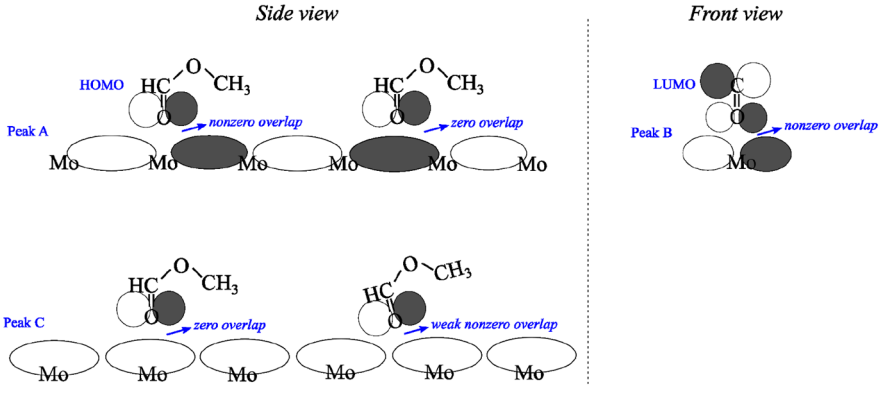


**Figure 6.** Schematic representation of the interaction between methyl formate HOMO−LUMO and Mo d bands. Gray and white lobes represent positive and negative phases, respectively. Peaks A, B, and C refer to d band peaks in Figure 2. Methyl formate could be strongly adsorbed at Mo-top via interaction between the HOMO and peak A, as well as the LUMO and peak B. Meanwhile, there should be a weak interaction between the HOMO and peak C on Mo−Mo-bridge.



https://doi.org/10.1021/acsomega.2c06888
ACS Omega 2023, 8, 6523−6529

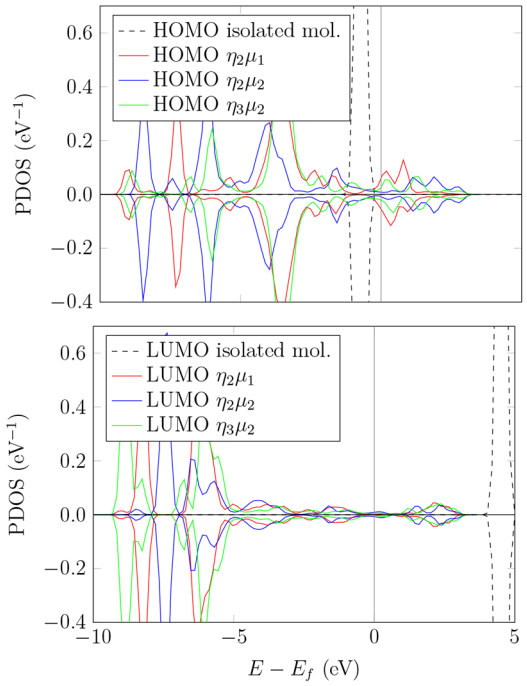


**Figure 7.** Projected density of states (PDOS) of the methyl formate's HOMO and LUMO, before and after adsorption. The energy level on the horizontal axis is relative to the Fermi level. The positive and negative values of PDOS correspond to spin up and down, respectively.

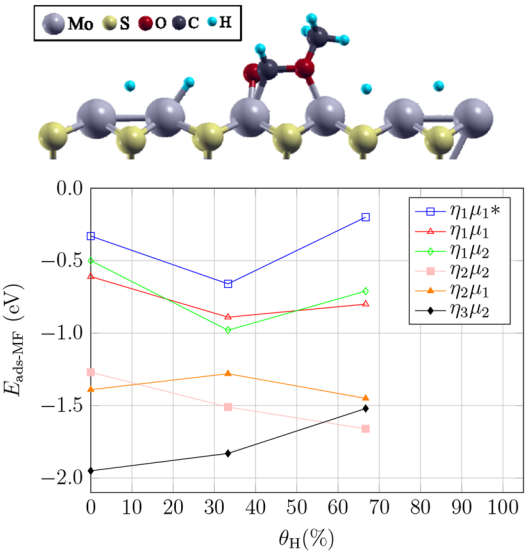


**Figure 8.** To see the effect of hydrogen coverage ($\theta_H$) on methyl formate adsorption energy ($E_{ads\text{-}MF}$), we put two hydrogen atoms on the right of the adsorbed methyl formate (corresponding to $\theta_H$ = 33.3%) and then the other two on the left ($\theta_H$ = 66.7%), as shown in the upper panel figure. The effect is shown in the lower panel figure.

$MoS_2$ surface. The Mo-edge has $d_{z^2}$, $d_{xz}$, and $d_{yz}$ peaks near the Fermi level, providing the adsorption sites on the surface's Mo-top and Mo−Mo-bridge. Since the symmetry of the frontier orbitals of hydrogen and methyl formate are different, they prefer to interact with different d bands. This results in different preferential adsorption sites of hydrogen and methyl formate; i.e., hydrogen prefers to be adsorbed on Mo−Mo-bridge, while methyl formate prefers Mo-top.

We observed that methyl formate could be adsorbed either in $\eta_1$, $\eta_2$, or $\eta_3$ mode. In the $\eta_1$ mode, methyl formate adsorbs weakly through its oxygen atoms with the adsorption energy more positive than −0.6 eV. On the other hand, the $\eta_2$ and $\eta_3$ modes involve a $\pi$ back-donation that stabilizes the adsorption at more than −1.0 eV.

Methyl formate and hydrogen receive electrons from $MoS_2$ upon adsorption. These excess electrons caused Coulombic repulsive interaction between the adsorbates. The interaction stabilizes their adsorption at low hydrogen coverage but later destabilizes it at high hydrogen coverage. The destabilization may cause desorption of $\eta_1$ modes of methyl formate due to its weak adsorption energy. Thus, at high hydrogen coverage, one may expect only $\eta_2$ or $\eta_3$ modes to exist on the surface.

## ■ ASSOCIATED CONTENT

### Supporting Information

The Supporting Information is available free of charge at https://pubs.acs.org/doi/10.1021/acsomega.2c06888.

Convergence test for k-point, kinetic energy cutoff, and vacuum height of the slab model; Bader change for the adsorbates; PDOS to the methyl formate's molecular orbital; optimized geometric parameters of adsorbed methyl formate; visualization of all methyl formate's adsorption modes in several variations of hydrogen coverage; hydrogen diffusion barriers; and methyl formate $\mu_1\eta_1$* into $\mu_3\eta_2$ energy barriers (PDF)

## ■ AUTHOR INFORMATION


### Corresponding Author

**Febdian Rusydi** − *Research Center for Quantum Engineering Design, Faculty of Science and Technology and Department of Physics, Faculty of Science and Technology, Universitas Airlangga, 60115 Surabaya, Indonesia;* orcid.org/0000-0002-7224-5731; Email: rusydi@fst.unair.ac.id

### Authors

**Samuel E. P. P. Masan** − *Department of Precision Engineering, Graduate School of Engineering, Osaka University, 565-0871 Osaka, Japan; Research Center for Quantum Engineering Design, Faculty of Science and Technology, Universitas Airlangga, 60115 Surabaya, Indonesia*

**Wahyu A. E. Prabowo** − *Research Center for Materials Informatics, Faculty of Computer Science, Universitas Dian Nuswantoro, 50131 Semarang, Indonesia; Research Center for Quantum Engineering Design, Faculty of Science and Technology, Universitas Airlangga, 60115 Surabaya, Indonesia;* orcid.org/0000-0003-4957-4331

**Daniel Elisandro** − *Research Center for Quantum Engineering Design, Faculty of Science and Technology, Universitas Airlangga, 60115 Surabaya, Indonesia*

**Wun F. Mark-Lee** − *Department of Chemistry, Faculty of Science, Universiti Teknologi Malaysia, 81310 Johor Bahru, Malaysia*

**Nabila A. Karim** − *Fuel Cell Institute, Universiti Kebangsaan Malaysia, 43600 Selangor, Malaysia*

**Adhitya G. Saputro** − *Advanced Functional Materials Research Group, Institut Teknologi Bandung, 40132 Bandung, Indonesia;* orcid.org/0000-0001-7848-3602

Complete contact information is available at: https://pubs.acs.org/10.1021/acsomega.2c06888




https://doi.org/10.1021/acsomega.2c06888
ACS Omega 2023, 8, 6523−6529

### Author Contributions

Conceptualization: Febdian Rusydi. Methodology: Febdian Rusydi and Samuel E. P. P. Masan. Validation: Wun F. Mark-Lee, Nabila A. Karim, and Adhitya G. Saputro. Formal Analysis: Samuel E. P. P. Masan, Wahyu A. E. Prabowo, Adhitya G. Saputro, Daniel Elisandro, and Febdian Rusydi. Investigation: Samuel E. P. P. Masan and Daniel Elisandro. Resources: Febdian Rusydi. Writing—original draft preparation: Samuel E. P. P. Masan. Writing—review and editing: Febdian Rusydi and Samuel E. P. P. Masan.

### Funding

This research is funded by "SATU Joint Research Scheme Universitas Airlangga Tahun 2021" number 1296/UN3.15/PT/2021.

### Notes

The authors declare no competing financial interest.

## ■ ACKNOWLEDGMENTS

All Quantum ESPRESSO calculations were performed in "Riven", the computational facility at the Research Center for Quantum Engineering Design, Universitas Airlangga. The authors thank Prof. Yoshitada Morikawa (Osaka University, Japan) for insightful and valuable discussions. S.E.P.P.M. thanks the Ministry of Education, Culture, Sports, Science, and Technology, Japan, for the Scholarship. S.E.P.P.M. thanks Rizka N. Fadilla (Osaka University, Japan) for the insightful discussions.

## ■ REFERENCES

(1) Sabatier, P. *La catalyse en chimie organique*;1920.
(2) Hammer, B.; Nørskov, J. K. Why gold is the noblest of all the metals. *Nature* **1995**, *376*, 238−240.
(3) Hammer, B.; Nørskov, J. K. Electronic factors determining the reactivity of metal surfaces. *Surf. Sci.* **1995**, *343*, 211−220.
(4) Hammer, B.; Morikawa, Y.; Nørskov, J. K. CO Chemisorption at Metal Surfaces and Overlayers. *Phys. Rev. Lett.* **1996**, *76*, 2141−2144.
(5) Bligaard, T.; Nørskov, J. K.; Dahl, S.; Matthiesen, J.; Christensen, C.; Sehested, J. The Brøsted-Evans-Polanyi relation and the volcano curve in heterogeneous catalysis. *J. Catal.* **2004**, *224*, 206−217.
(6) Lausche, A. C.; Medford, A. J.; Khan, T. S.; Xu, Y.; Bligaard, T.; Abild-Pedersen, F.; Nørskov, J. K.; Studt, F. On the effect of coverage-dependent adsorbate-adsorbate interactions for CO methanation on transition metal surfaces. *J. Catal.* **2013**, *307*, 275−282.
(7) Li, J.; Fleurat-Lessard, P.; Zaera, F.; Delbecq, F. Mechanistic investigation of the cis/trans isomerization of 2-butene on Pt(111): DFT study of the influence of the hydrogen coverage. *J. Catal.* **2014**, *311*, 190−198.
(8) Wang, S.; Vorotnikov, V.; Vlachos, D. G. Coverage-Induced Conformational Effects on Activity and Selectivity: Hydrogenation and Decarbonylation of Furfural on Pd(111). *ACS Catal.* **2015**, *5*, 104−112.
(9) Huang, X.; Cant, N.; Evans, J.; Wainwright, M. Kinetic studies of gas-phase hydrogenolysis of methyl formate to methanol over copper-based catalyst. *Catal. Today* **2004**, *93*−*95*, 113−119. Selections from the presentations of the third Asia-Pacific Congress on Catalysis.
(10) Wang, W.; Tan, S.; Wu, K.; Zhu, G.; Liu, Y.; Tan, L.; Huang, Y.; Yang, Y. Hydrodeoxygenation of p-cresol as a model compound for bio-oil on $MoS_2$: Effects of water and benzothiophene on the activity and structure of catalyst. *Fuel* **2018**, *214*, 480−488.
(11) Grønborg, S. S.; Salazar, N.; Bruix, A.; Rodríguez-Fernández, J.; Thomsen, S. D.; Hammer, B.; Lauritsen, J. V. Visualizing hydrogen-induced reshaping and edge activation in MoS2 and Co-promoted $MoS_2$ catalyst clusters. *Nat. Commun.* **2018**, *9*, 2211.
(12) Kronberg, R.; Hakala, M.; Holmberg, N.; Laasonen, K. Hydrogen adsorption on $MoS_2$-surfaces: a DFT study on preferential sites and the effect of sulfur and hydrogen coverage. *Phys. Chem. Chem. Phys.* **2017**, *19*, 16231−16241.
(13) Rosen, A. S.; Notestein, J. M.; Snurr, R. Q. Comprehensive Phase Diagrams of $MoS_2$ Edge Sites Using Dispersion-Corrected DFT Free Energy Calculations. *J. Phys. Chem. C* **2018**, *122*, 15318−15329.
(14) Sotelo-Boyás, R.; Trejo-Zárraga, F.; de Jesús Hernández-Loyo, F. In *Hydrogenation*; Karamé, I., Ed.; IntechOpen: Rijeka, 2012; Chapter 8.
(15) Srifa, A.; Faungnawakij, K.; Itthibenchapong, V.; Assabumrungrat, S. Roles of monometallic catalysts in hydrodeoxygenation of palm oil to green diesel. *Chem. Eng. J. (Amsterdam, Neth.)* **2015**, *278*, 249−258. Tailoring Sustainability through Chemical Reaction Engineering.
(16) Cheah, K. W.; Yusup, S.; Loy, A. C. M.; How, B. S.; Skoulou, V.; Taylor, M. J. Recent advances in the catalytic deoxygenation of plant oils and prototypical fatty acid models compounds: Catalysis, process, and kinetics. *Mol. Catal.* **2022**, *523*, 111469.
(17) Wan Khalit, W. N. A.; Asikin-Mijan, N.; Marliza, T. S.; Safa-Gamal, M.; Shamsuddin, M. R.; Azreena, I. N.; Saiman, M. I.; Taufiq-Yap, Y. One-pot decarboxylation and decarbonylation reaction of waste cooking oil over activated carbon supported nickel-zinc catalyst into diesel-like fuels. *J. Anal. Appl. Pyrolysis* **2022**, *164*, 105505.
(18) Abelniece, Z.; Laipniece, L.; Kampars, V. Biodiesel production by interesterification of rapeseed oil with methyl formate in presence of potassium alkoxides. *Biomass Convers. Biorefin.* **2022**, *12*, 2881−2889.
(19) Makareviciene, V.; Sendzikiene, E.; Gaide, I.; Kazancev, K. Application of methyl formate in the process of biotechnological interesterification of triglycerides for the production of biodiesel. *Biomass Conversion and Biorefinery* **2022**, DOI: 10.1007/s13399-022-03390-4.
(20) Prabowo, W. A. E.; Subagjo; Nugraha; Agusta, M. K.; Saputro, A. G.; Rustad, S.; Maezono, R.; Diño, W. A.; Dipojono, H. K. Density functional study of methyl butanoate adsorption and its C−O bonds cleavage on $MoS_2$-based catalyst with various loads of Ni promoters. *J. Phys.: Condens. Matter* **2019**, *31*, 365001.
(21) Giannozzi, P.; et al. QUANTUM ESPRESSO: a modular and open-source software project for quantum simulations of materials. *J. Phys.: Condens. Matter* **2009**, *21*, 395502.
(22) Giannozzi, P.; et al. Advanced capabilities for materials modelling with Quantum ESPRESSO. *J. Phys.: Condens. Matter* **2017**, *29*, 465901.
(23) Dal Corso, A. Pseudopotentials periodic table: From H to Pu. *Comput. Mater. Sci.* **2014**, *95*, 337−350.
(24) Perdew, J. P.; Burke, K.; Ernzerhof, M. Generalized Gradient Approximation Made Simple. *Phys. Rev. Lett.* **1996**, *77*, 3865−3868.
(25) Grimme, S. Semiempirical GGA-type density functional constructed with a long-range dispersion correction. *J. Comput. Chem.* **2006**, *27*, 1787−1799.
(26) Bronsema, K. D.; De Boer, J. L.; Jellinek, F. On the structure of molybdenum diselenide and disulfide. *Z. Anorg. Allg. Chem.* **1986**, *540*, 15−17.
(27) Monkhorst, H. J.; Pack, J. D. Special points for Brillouin-zone integrations. *Phys. Rev. B* **1976**, *13*, 5188−5192.
(28) Fletcher, R. *Practical Methods of Optimization*, 2nd ed.; John Wiley & Sons: New York, 1987; p 49−57.
(29) Ravikumar, A.; Baby, A.; Lin, H.; Brivio, G. P.; Fratesi, G. Femtomagnetism in graphene induced by core level excitation of organic adsorbates. *Sci. Rep.* **2016**, *6*, 14603.
(30) Henkelman, G.; Uberuaga, B. P.; Jónsson, H. A climbing image nudged elastic band method for finding saddle points and minimum energy paths. *J. Chem. Phys.* **2000**, *113*, 9901−9904.
(31) Tang, W.; Sanville, E.; Henkelman, G. A grid-based Bader analysis algorithm without lattice bias. *J. Phys.: Condens. Matter* **2009**, *21*, 084204.
(32) Wilmshurst, J. A vibrational assignment for methyl formate and methyl acetate. *J. Mol. Spectrosc.* **1957**, *1*, 201−215.
(33) Müller, R.; Hollenstein, H.; Huber, J. Light-induced isomerization and photochemical transformation of methylformate in an


https://doi.org/10.1021/acsomega.2c06888
ACS Omega 2023, 8, 6523−6529

argon matrix. Vibrational frequencies, force field, and normal coordinate analysis of trans-methylformate. *J. Mol. Spectrosc.* **1983**, *100*, 95−118.
(34) Tománek, D.; Wilke, S.; Scheffler, M. Hydrogen-Induced Polymorphism of the Pd(110) Surface. *Phys. Rev. Lett.* **1997**, *79*, 1329−1332.
(35) Li, W.-X.; Stampfl, C.; Scheffler, M. Subsurface oxygen and surface oxide formation at Ag(111): A density-functional theory investigation. *Phys. Rev. B* **2003**, *67*, 045408.
(36) Mortensen, P.; Grunwaldt, J.-D.; Jensen, P.; Knudsen, K.; Jensen, A. A review of catalytic upgrading of bio-oil to engine fuels. *Appl. Catal., A* **2011**, *407*, 1−19.
(37) Dupont, C.; Lemeur, R.; Daudin, A.; Raybaud, P. Hydrodeoxygenation pathways catalyzed by $MoS_2$ and NiMoS active phases: A DFT study. *J. Catal.* **2011**, *279*, 276−286.
(38) Ruinart de Brimont, M.; Dupont, C.; Daudin, A.; Geantet, C.; Raybaud, P. Deoxygenation mechanisms on Ni-promoted $MoS_2$ bulk catalysts: A combined experimental and theoretical study. *J. Catal.* **2012**, *286*, 153−164.
(39) Salciccioli, M.; Edie, S. M.; Vlachos, D. G. Adsorption of Acid, Ester, and Ether Functional Groups on Pt: Fast Prediction of Thermochemical Properties of Adsorbed Oxygenates via DFT-Based Group Additivity Methods. *J. Phys. Chem. C* **2012**, *116*, 1873−1886.
(40) Valencia, D.; García-Cruz, I.; Ramírez-Verduzco, L. F.; Aburto, J. Adsorption of Biomass-Derived Products on MoO3: Hydrogen Bonding Interactions under the Spotlight. *ACS Omega* **2018**, *3*, 14165−14172.





https://doi.org/10.1021/acsomega.2c06888
*ACS Omega* 2023, 8, 6523−6529